Article

The Mechanism of Phase Transfer Synthesis of Silver Nanoparticles Using a Fatty Amine as Extractant/Phase Transfer Agent

Konrad Wojtaszek [1], Tomasz Tokarski [2], Dawid Kutyła [1], Karolina Kołczyk-Siedlecka [1], Piotr Żabiński [1], Edit Csapó [3], Robert P. Socha [4], Marc Escribà-Gelonch [5], Volker Hessel [6,7] and Marek Wojnicki [1,*]

1   Faculty of Non-Ferrous Metals, AGH University of Science and Technology, Mickiewicza Ave. 30, 30-059 Krakow, Poland
2   Academic Centre for Materials and Nanotechnology, AGH University of Science and Technology, al. A. Mickiewicza 30, 30-059 Krakow, Poland
3   MTA-SZTE "Lendület" Momentum Noble Metal Nanostructures Research Group, University of Szeged, Rerrich B. sqr. 1, H-6720 Szeged, Hungary
4   CBRTP SA Research and Development Center of Technology for Industry, Ludwika Waryńskiego 3A, 00-645 Warszawa, Poland
5   Higher Polytechnic Engineering School, Department of Chemistry, University of Lleida, 08700 Igualada, Spain
6   School of Engineering, University of Warwick, Coventry CV4 7AL, UK
7   School of Chemical Engineering, The University of Adelaide, Adelaide, SA 5005, Australia
*   Correspondence: marekw@agh.edu.pl

Abstract: The paper presents the research results on synthesizing silver nanoparticles in aqueous solutions and their extraction into the organic phase. Studies have shown that it is best to perform the extraction process using n-hexane > cyclohexane > toluene > chloroform > ethyl acetate. The results show a correlation between the dielectric constant of the organic phase and its ability to extract nanoparticles. The lower the dielectric constant is, the higher the extractability. The hydrodynamic radius of the silver nanoparticles changes after transfer to the organic phase, depending greatly on the organic phase used. The extraction mechanism is complex and multi-step. As the first step, the Ag nanoparticles are transferred to the phase boundary. As the second step, the octadecylamine (ODA) molecules adsorb on the silver nanoparticles (AgNPs) surface. The change in particle shape was also noted. This suggests that the interfacial processes are more complex than previously reported. Below the initial concentration of ODA 2×10^{-4} M, the formation of a third phase has been observed. In a one-stage experiment, the concentration of silver nanoparticles after transferring to the organic phase was increased 500 times in about 10 s. The role of the concentration of ODA, therefore, is not only a measure of the extraction efficiency and productivity but functions as an enabler to maintain favorable biphasic processing, which underlines the role of the solvent again.

Keywords: nanoparticles; silver; phase transfer; extraction; mass production

1. Introduction

The synthesis of silver nanoparticles is an important issue. There are a variety of methods for synthesizing silver nanoparticles [1]. The main methods are physical [2] and chemical [2,3]. Physical methods include laser ablation [4], sputtering [5], and electrical discharge [6]. Chemical methods include chemical reduction [7], microwave-assisted reduction [8–10], electrochemical reduction [11], and photochemical reduction [12,13]. In the chemical reduction method, silver ions are reduced by a reducing agent. This is the most widely used method to produce silver nanoparticles. In the electrochemical reduction method, silver ions are reduced by an electric current [14–17]. In the photochemical reduction method, silver ion reduction process is catalyzed by light. Chemical methods are generally preferred in synthesizing silver nanoparticles due to their higher efficiency,

lower cost, and ability to control the size and shape of the nanoparticles. The most common chemical-reducing agents used for this purpose are sodium borohydride [18,19], citric acid, ascorbic acid [20–23], glucose [24], and borane dimethylamine complex [25,26]. Variations of these reducing agents are also used. The size and shape of the silver nanoparticles can be controlled by varying the reducing agent [27–29], reaction temperature [30], solution pH [31], and reaction time [32–34]. The size of the nanoparticles can also be adjusted by post-synthesis treatments such as sonication [35] and centrifugation.

Typically, colloids obtained by the above methods have concentrations too low for practical applications or even analytical purposes. To increase the concentration of colloidal suspension, several methods can be used, such as: Centrifugation, ultrafiltration, precipitation, and evaporation. The centrifugation method is used to separate the solid particles from the liquid in a suspension by spinning the suspension at high speed in a centrifuge [36]. This method has many disadvantages. Particles with a strong surface charge are practically not centrifuged. The electrostatic forces are too great. In the case of particles stabilized with polymers with a low surface charge, the centrifugal force may be too high and lead to the particles joining into larger agglomerates. Another alternative concentration method is ultrafiltration, which is used to separate the particles in a suspension based on size by forcing the liquid through a membrane [37]. The main disadvantage of this method is that these membranes are costly. In addition, filtration at the level of 10 nm requires huge pressures, which is associated with increased costs. The typical method for preconcentration is precipitation: This is used to increase the concentration of a colloidal suspension by adding a precipitating agent, such as a strong acid or alkaline, to the suspension. However, the reaction often leads to aggregation and growth of nanoparticles. That changes their physical and chemical properties.

All those methods are complex, time-consuming, and often require specialized equipment. Therefore, continuing innovation is required. A solution to this problem is provided by evaporation, which has been demonstrated to be a simple and well-known method of concentration by evaporation of the dispersant. This process does not require specialized equipment, is universal and one-stage. This method works well when the colloid is stabilized with a polymer. In the case of colloids stabilized by a surface charge, the salinity increase due to the evaporation of the dispersant leads to a decrease in the zeta potential. As a result, the colloid loses its stability. The solution may be to use dialysis and evaporation in parallel, involving significant energy costs. The literature has reported on an alternative via using ODA to transfer nanoparticles from the aqueous phase to the organic phase [38–40]. The number of respective publications has increased rapidly recently, but the mechanism of action of ODA was not studied in detail but rather presented as a curiosity [41]. Therefore, this work aims to investigate the interfacial transfer mechanism of silver nanoparticles.

2. Experimental

At the beginning, silver nanoparticles were synthesized as follows: An aqueous solution of silver(I) nitrate (A.P., POCH, Gliwice, Poland) with a concentration 5×10^{-4} M was prepared. Next, an aqueous solution of tri-sodium citrate (TSC) (Pure, POCH, Gliwice, Poland) with a concentration 5×10^{-4} M was prepared. These two solutions have high chemical stability, therefore, they can be stored for longer than 24 h. In the case of silver nitrate, it should be protected from sunlight. Finally, sodium borohydride (99%, Acros, Gell, Belgium) solution was prepared. This reagent is characterized by high chemical instability in aqueous solutions. Therefore, we recommend preparing the solution directly before performing the experiment. It may be helpful to prepare a much higher concentration solution and then dilute it immediately before the experiments. Nanoparticle synthesis was performed at the Erlenmeyer flask. A magnetic stirrer was placed at the bottom of the reaction vessel. The size of the stirrer bar and the speed of rotation should be chosen to ensure a quick mixing of reactants. In our case, the magnetic stirrer size was 2 cm, and the mixing rate was 1000 rpm. The volume of the Erlenmeyer flask was 150 mL. Next, 50 mL of $AgNO_3$ and 50 mL of TSC were mixed. After c.a. 20 s, 3 mL of the solution containing

NaBH$_4$ was added. The color of the solution changed quickly to yellow. After c.a. 5 min, reaction stopped, and the final color was dark yellow. This colloid was later used in all experiments. The solutions were prepared using demineralized water with conductivity σ = 0.05 μS (Polwater DL3N-150, Kraków, Poland).

The octadecyl amine, also known as fatty amine (ODA) (MERCK, 90%) solution with the concentration of 8×10^{-4} M was prepared in five different, non-polar solvents. As a solvent, n-hexane (POCH, A.P.), cyclohexene (POCH, A.P.), chloroform (POCH, A.P.), ethyl acetate (POCH, A.P.), and toluene (POCH, A.P.) were used.

The UV–Vis spectra of the obtained AgNPs were examined using a Shimadzu UV–2401 PC spectrophotometer (Shimadzu Corp., Tokyo, Japan) in the 200–900 nm range. Quartz cuvettes were used (Hellma Analytics, Müllheim, Germany). The particle size distribution and Zeta potential in the obtained colloids were measured by DLS (Dynamic Light Scattering) using Malvern Instruments Zetasizer Nano (Malvern Panalytical, Malvern, UK) (laser 633 nm). The FTIR study for the synthesized nanoparticles was carried out on a Nicolet 380 FT-IR Spectrometer (Thermo Scientific, Waltham, MA, USA) in the range of 500–4000 cm^{-1} using a solid sample holder. Preparation of the sample for FT-IR measurement consisted in dripping 200 μL of colloid into a portion of potassium bromide, (IR grade 99+%, Merck, Darmstadt, Germany), then evaporation at 70 °C for 30 min, then grinding in an agate mortar and pressing in a matrix with a diameter of 10 mm at a pressure of 150 atm using a hydraulic press. The pellets prepared in this way were measured for transmittance. HR–TEM analysis was performed using FEI TECNAI TF 20 X–TWIN microscope (Thermo Fisher Scientific, Bremen, Germany). For this purpose, AgNPs colloidal suspension was placed on a copper grid covered with a 20–30 nm amorphous carbon film. Then, the sample was left to dry at room temperature (ca. 20 °C).

Images from the HR-TEM were analyzed using several steps of protocol related to image preparation. For this purpose, ImageJ software version 1.52v was used. First, the scale was digitalized. Next, the image was cut to remove the scale bar as well as the text boxes. Next, the image was filtered using the FFT bandpass filter. The settings of the filter were as follows: Filter large structures down to 40 pixels, filter small structures up to 3 pixels, suppress stripes none, tolerance of direction 5%. Next, the particle size was determined as follows: Using threshold setup, alloy nanoparticles were detected, and the image was converted to black–white. Using the analysis particles tool, carbon quantum dots' surface areas were determined. The following parameters were selected: size nm^2 from 1 to infinity. This allows removing single pixels and artifacts from the image. Next, circularity was selected in the range of 0.5–1. This allows excluding from analysis particles that are stuck together. The diameter was calculated at and from the surface area of single carbon quantum dots, and the histograms were plotted.

XRD analysis was performed using the Rigaku MiniFlex instrument (Tokyo, Japan). For this purpose, obtained colloids were evaporated on the glass substrate. Next, obtained deposit on the glass substrate was analyzed. To obtain a sufficient amount of materials, 10 mL of the sample was evaporated.

The analysis of UV-Vis spectra was carried out using the Spectragryph software (Oberstdorf, Germany, Dr. Friedrich Menges Software-Entwicklung).

3. Results and Discussion

ODA is insoluble in water but soluble in various aprotic solvents. Figure 1 presents photographs of the samples before and after extraction of silver nanoparticles from the water phase to the organic phase, demonstrating color changes of the liquids and solid materials precipitation.

The numbers from 1 to 5 denote solvents: 1—chloroform, 2—n-hexane, 3—toluene, 4—cyclohexane, 5—ethyl acetate. It should be noted that, in the case of chloroform, the density of the organic phase is higher than the water phase, therefore, yellow colloids are at the top of the test tube. In other cases, the water part is at the bottom of the test tubes.
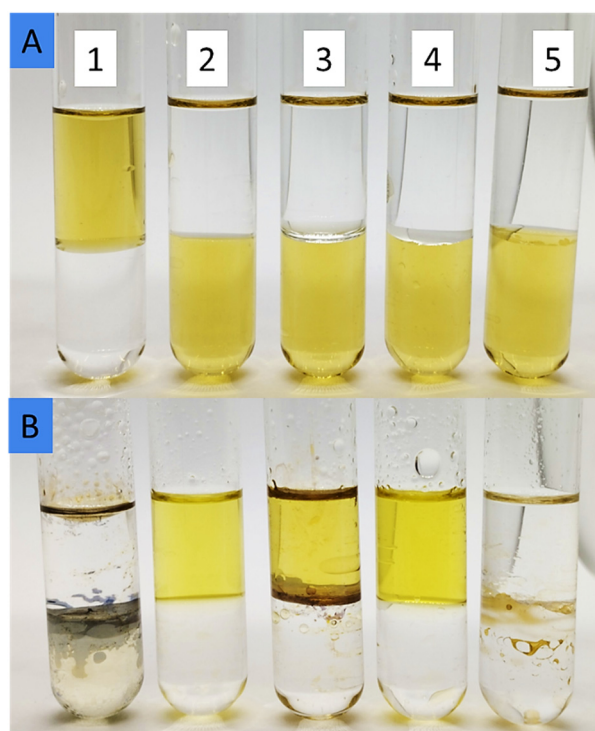
Figure 1. View of the samples (**A**) before extraction, (**B**) after extraction.

As can be observed, in the case of chloroform, toluene, and ethyl acetate, a third phase was formed. As can be seen in Figure 1B, the precipitated third phase takes the form of a thin film. The color of the thin film depends on the organic phase type, ranging from beige (ethyl acetate) and dark brown (toluene) to dark gray (chloroform). The precipitate tends to stick to the glass wall of the test tube.

This points to the insolubility of the third phase in either the aqueous or organic phases. Water and organic phases were analyzed using several methods to confirm the efficiency of AgNPs extraction.

3.1. UV-Vis Analysis

UV-Vis analysis of the organic and water phase after extraction was performed, Figure 2. The UV-Vis spectrum of AgNPs shown in Figure 2A was taken immediately after synthesis.
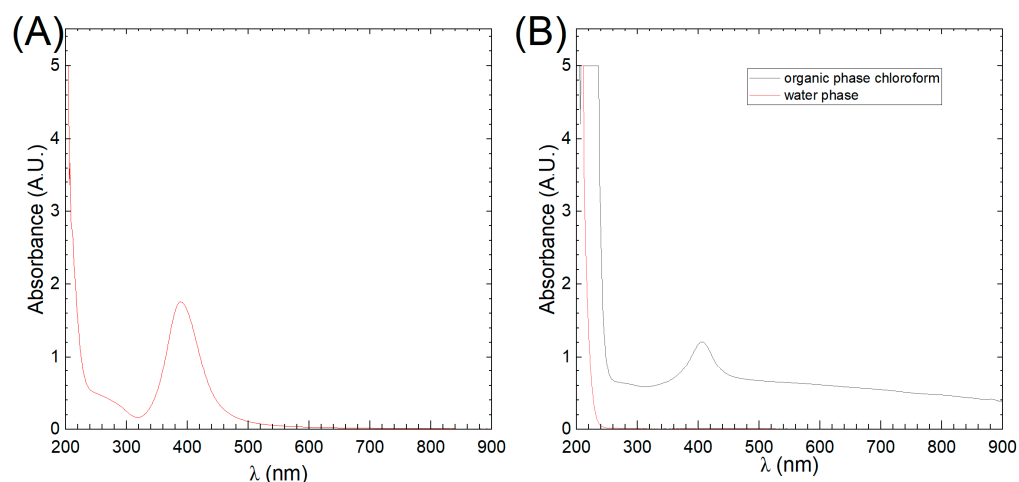
Figure 2. *Cont.*
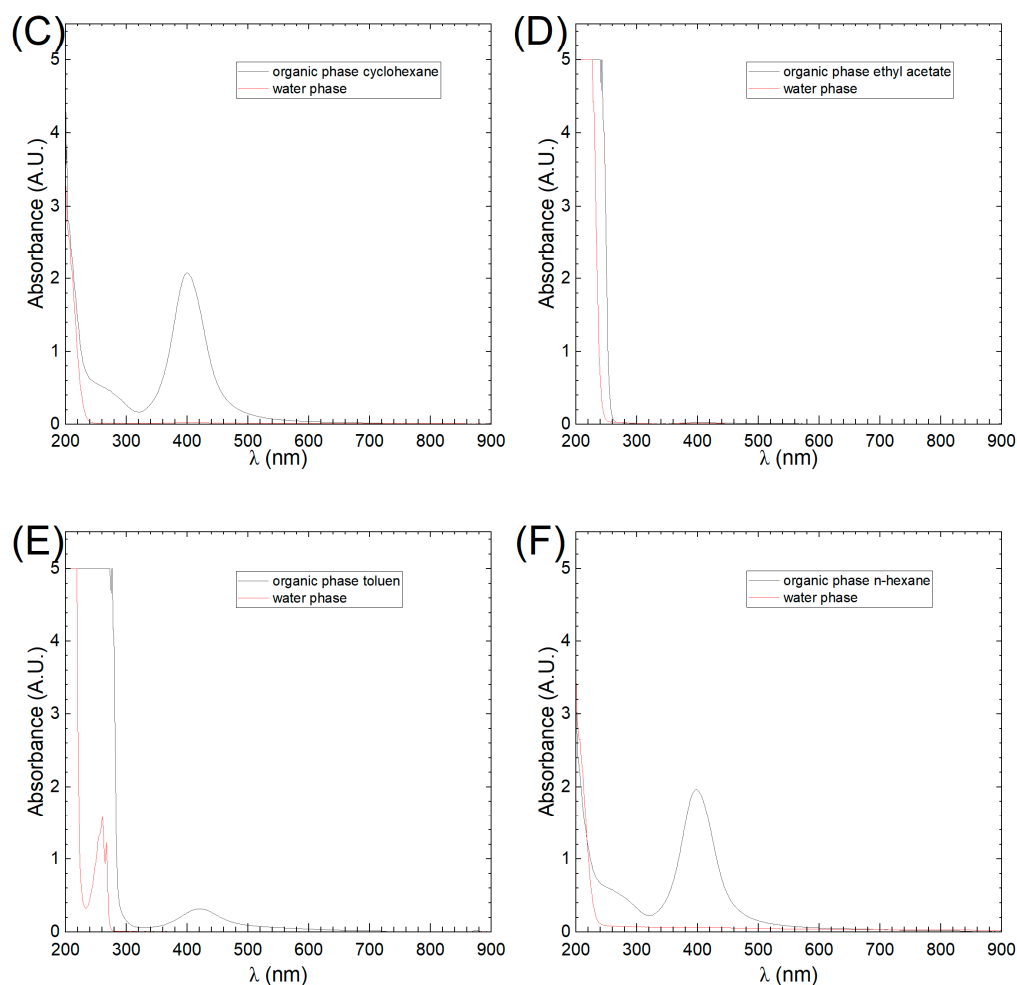
Figure 2. UV-Vis spectrum of samples (**A**) AgNPs directly after synthesis, (**B–F**) organic and water phase after extraction to different solvents.

Before extraction (Figure 2A), an absorption peak with a maximum at 389 nm is observed in the aqueous solution. This peak is related to the plasmon resonance occurring in the silver nanoparticle. The location and shape of this file are directly related to the size of the nanoparticles. Typically, smaller nanoparticles absorb shorter wavelengths, while larger nanoparticles absorb longer wavelengths. It is also well known that the surface plasmon resonance of silver nanoparticles depends on the dispersed phase composition. This is due to the direct interaction of the dispersant and the stabilizer with the plasmonic wave in the nanoparticle. Therefore, after the extraction of silver nanoparticles from the aqueous phase to the organic phase, a slight shift in the peak position due to the change of the dispersant can be expected (see Figure 2B–F). Table 1 compiles data about the absorption band position maximum, as well as the absorbance level in the organic phase and extraction efficiency. Additionally, the dielectric constants for all dispersants are gathered.

Table 1. AgNPs extraction efficiency and absorption peak position and intensity.

AgNPs in Different Solvents	λ_{max}, nm	Absorbance Organic Phase, A.U.	Extraction Efficiency, %	Dielectric Constant ε, -	Solubility of Dispersant Phase in Water, mg/L
water	389	1.757	100.0	80.1	No limit
n-hexane	399	1.962	100.0	2.1	9.5
cyclohexene	400	2.077	98.5	2.2	55
toluene	420	0.315	100.0	2.4	526
chloroform	406	1.209	100.0	4.8	7.95×10^3
ethyl acetate	408	0.03	98.9	6.0	64×10^3

The extraction efficiency was calculated using Equation (1):

$$E_{ef} = \frac{C_0 - C_r}{C_0} \cdot 100\% \tag{1}$$

where:

E_{ef}—extraction efficiency, %

C_0—initial concentration of colloid in the water phase, g/L

C_r—concentration of colloid in the water phase after extraction at the equilibrium state, g/L

As can be seen, the peak position changes depending on the organic phase. As mentioned earlier, the change in the peak position may be related to the change in the dispersing phase. Moreover, the absorbance level also depends on the organic solvent. The highest absorbance was measured for AgNPs in cyclohexene and n-hexane. It is worth noting that only in these two cases, the third phase was not observed. In all the cases, the extraction from water phase efficiency was high and exceeded 95%.

A large gap in dielectric permittivity is provided between water and the organic solvent used. This facilitates particle transfer via the water/oil interface. The stabilizing agent ODA adsorbs at the particle surface leading to cross-linking [42]. The new surface created by this coating allows dissolution in the organic solvent, which can finally form a third phase composed of NPs covered and linked by ODA. It should be noted that a small change in the dielectric constants of the organic solvent causes a significant increase in the solubility of this compound in water. For this reason, this study was restricted to a narrow range of dielectric constants of organic solvents.

Dissolved organic compounds in water change it dielectric permittivity. The dielectric permittivity change as a function of the mole fraction of the dissolved compound, e.g., organic compound [43]. The larger the difference between the dielectric constants at the interface, the larger the shift of the surface charge on the nanoparticle at the water/oil interface is observed. Charged spherical nanoparticles trapped at the interface between water and oil exhibit repulsive electrostatic forces that contain a long-ranged dipolar and a short-ranged exponentially decaying component. The former is induced by the unscreened electrostatic field through the non-polar low-permittivity medium and the latter result from the overlap of the diffuse ion clouds that form in the aqueous phase close to the nanoparticles. The magnitude of the long-ranged dipolar interaction is largely determined by the residual charges that remain attached to the oil-exposed region of the nanoparticle [44]. As a result, ODA tends to adsorbed on the oil side surface. To make this part clearer, we demonstrate it in Figure 3, where $\varepsilon_{n\text{-hexene}}$, ε_{water}, and ε_{AgNPs} denote dielectric constants of n-hexane, water, and silver nanoparticles, respectively. The surface charge densities of the particle at its n-hexene-exposed and water-exposed regions are denoted by σ_a and σ_w, respectively.
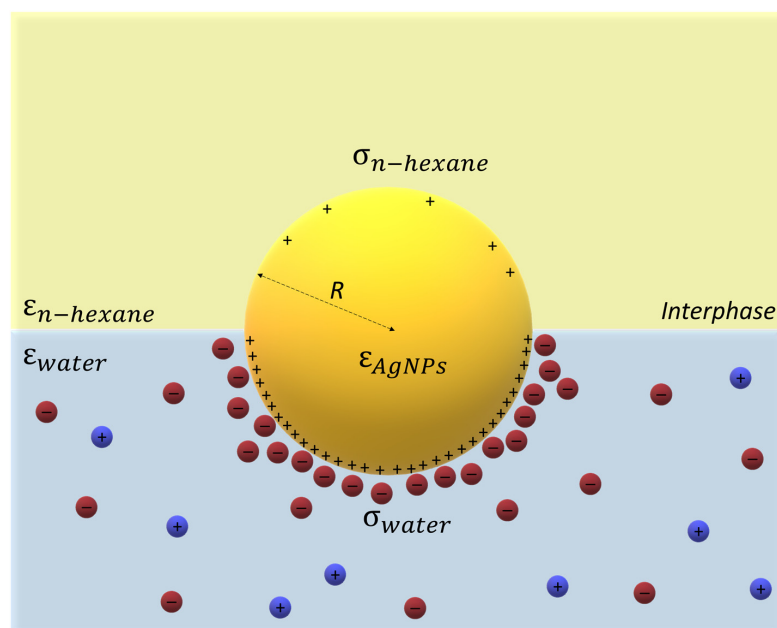
Figure 3. Schematic illustration of charged silver nanoparticles located at the interface between water and oil.

It should also be noted that when the extraction process starts, at the interphase, diffusion of water to oil and oil to water takes place. Intensive shaking makes obtaining a fast concentration equilibrium between water and oil possible. Thus, the final dielectric constant of the water and oil phase is different from what is given in the literature. When we compare the solubility of toluene and cyclohexane, we see that there is one order of magnitude difference in the solubility. Therefore, the final dielectric constants at the equilibrium state are significantly different from those given in the literature for pure solvents. This explains why a slight difference in dielectric constants of pure solvents gives a significant difference in final observations.

3.2. DLS-Analysis

For DLS analysis, the ethyl acetate phase was not taken into account since the UV-Vis analysis showed no absorption band of AgNPs in the organic phase. In the case of chloroform, a low intensive peak was detected. The determined diameter of nanoparticles is listed in Table 2.

Table 2. AgNPs diameter determined in different solvents.

AgNPs in Different Solvents	d, nm	SD, nm
water	22.0	2.8
n-hexane	20.3	0.8
cyclohexene	15.0	1.1
toluene	199.4	9.9
chloroform	11.6	1.6

In the case of water as the solvent, the zeta potential was determined as equal to -35 ± 5 mV. The presence of a strongly negative surface charge improves much stability of AgNPs in water. The surface charge is directly related to the presence of TSC, which undergoes dissociation in aqueous solutions and adsorption on the surface of Ag nanoparticles.

In the case of chloroform, a weak signal from the sample was registered. Therefore, the determined diameter may consist of significant error, or the extraction process, in this

case, is size-selective [43]. This last is rather unlikely. In the case of toluene, a significant increase in the size of AgNPs was noted. Moreover, significant changes in the intensity of the UV-Vis spectra peak were observed. This suggests that a "flocculation" process takes place in the organic phase. In the case of small molecules like ODA, flocculation is practically impossible. Flocculation occurs when long polymer chains entangle each other. However, in non-polar solvents, hydrogen bonding can be formed, so the ODA molecules can link to each other and form larger structures. Therefore, the calculated value from DLS is significantly higher.

3.3. FT-IR Analysis

FT-IR analysis was carried out for all samples for the extraction process from the aqueous phase to the organic phase containing ODA. The obtained spectra are presented in Figure 4. The first two spectra (red and green lines) represent the reference reagents, i.e., TSC and ODA, respectively. The remaining spectra are similar to the ODA reference spectrum. For extraction solvents, where a third phase was formed (ethyl acetate, chloroform), peaks are practically invisible.
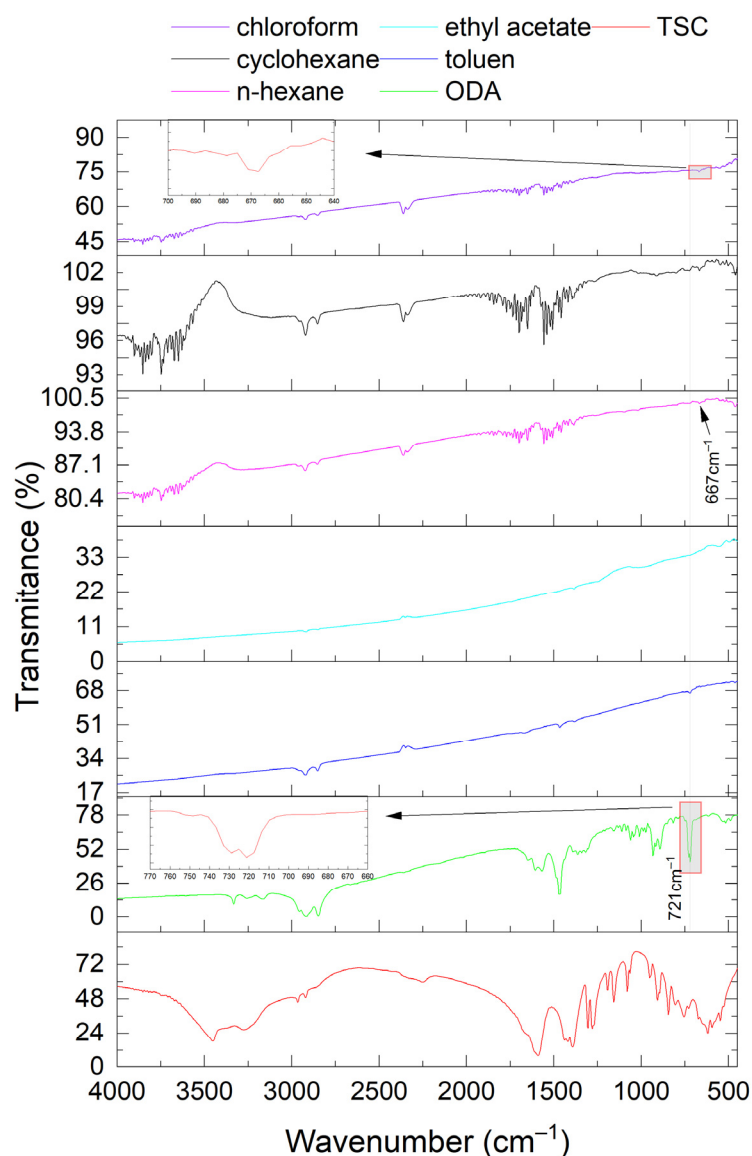

Figure 4. FT-IR analysis of AgNPs after the extraction process.

All spectra (except for the process using the solvent ethyl acetate) show peaks at 2923 and 2851 cm^{-1}. They are related to C-H$_{st}$ (stretching frequencies) bonds by interactions. Since the chain of the ODA molecule composed of these C-H$_{st}$ bonds is not involved in AgNPs extraction, there is no spectral change in this range. The difference in the lower wave numbers, in the range of 721 cm^{-1}, is clearly visible. It can be attributed to the C-N interaction in the amino group. This peak does not disappear but shifts very strongly for all samples. In the case of chloroform, its maximum is 666 cm^{-1}, while in hexane, it is 667 cm^{-1}. Such significant shifts may indicate a strong interaction between nitrogen (amine group) and silver. The lack of a clear change in the FT-IR spectra is due to the high concentration of unbound ODA in relation to the adsorbed ODA.

3.4. Influence of ODA Initial Concentration in N-Hexane

ODA acts as a phase transfer agent during the extraction of Ag nanoparticles into the organic phase. This ODA molecule consists of a long hydrophobic tail and is a primary alkyl amine mainly used as a hydrophobic surface modifier [45]. The presence of an amine functional group allows this molecule to adsorb at the surface of AgNPs effectively. However, the mechanism of the nanoparticle transfers is not clear. Figure 5 shows the influence of ODA initial concentration in the organic phase on the process of AgNPs extraction. The effect of solvent type was tested at a constant ODA concentration of 8×10^{-4} M. Subsequent studies were conducted for lower ODA concentrations.
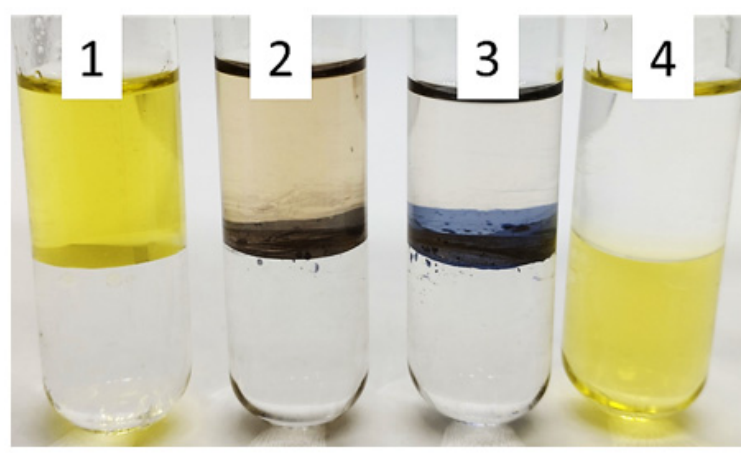
Sample No.	ODA Initial Concentration, M
1	4×10^{-4}
2	1.6×10^{-4}
3	8×10^{-5}
4	8×10^{-6}

Figure 5. Influence of ODA initial concentration in the organic phase (n-hexane) on the efficiency of extraction.

Below concentration 4×10^{-4} M, the third phase formation is observed. However, all AgNPs are removed from the water phase.

Further lowering of the concentration leads to complete inhibition of the AgNPs extraction process. This is unexpected because it seems to contradict the Nernst division law. It would be expected that as the ODA concentration in the organic phase decreases, the partition coefficient is proportional to the ODA concentration. It has to be noted that

the Nernst equation applies to small molecules, not to colloidal systems. Therefore, we performed further experiments to shed light on this problem.

3.5. Influence of Organic-Water Phase Ratio

The extraction of AgNPs to the organic phase offers process opportunities, including concentrating the colloid. The organic phase evaporates at a lower temperature than the water phase, which avoids thermally induced destruction of the colloid. Previous tests (Section 3.4) have shown that there is a critical concentration of ODA in the organic phase beyond which AgNPs cannot be extracted. We conducted a study in that various volume proportions of the organic phase of the water phase were mixed together, Figure 6.

Sample No.	Volume Ratio mL:mL	Extraction Efficiency, %
1	5:4	100
2	5:3	100
3	5:0.1	100
4	5:0.01	100
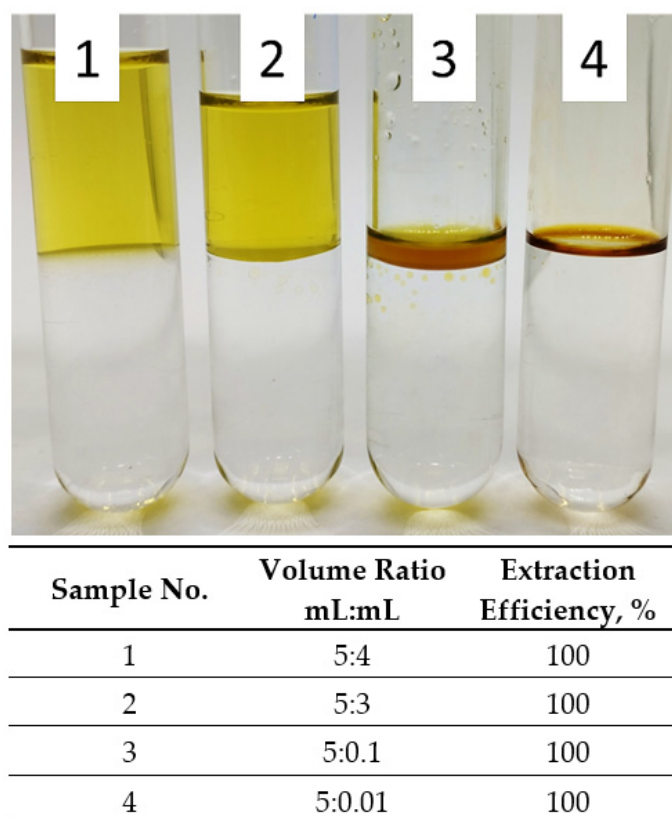
Figure 6. Influence of organic-water phase ratio.

In each case, silver nanoparticles were completely removed from the water phase. As a result, the aqueous phase becomes discolored, while the organic phase acquires an intense yellow color to brown notes depending on the volume of this organic phase.

If we assume that a simple reaction takes place between ODA and the AgNPs surface, in which the amine combines with the Ag, the change in the volume of the aqueous phase in relation to the organic phase should lead to the same results as reported for previous experiments, regarding the effect of the initial concentration of ODA on the extraction process. Surprisingly, when 0.01 mL of 8×10^{-4} M ODA was used, the amount of ODA was much less than in the experiment where 8×10^{-6} M ODA and 5 mL of the solution were used. In the first case, complete extraction took place, while in the second, a third phase was formed. It is hypothesized that the process is diffusion controlled. We have schematically presented the process of AgNPs extraction in Figure 7.
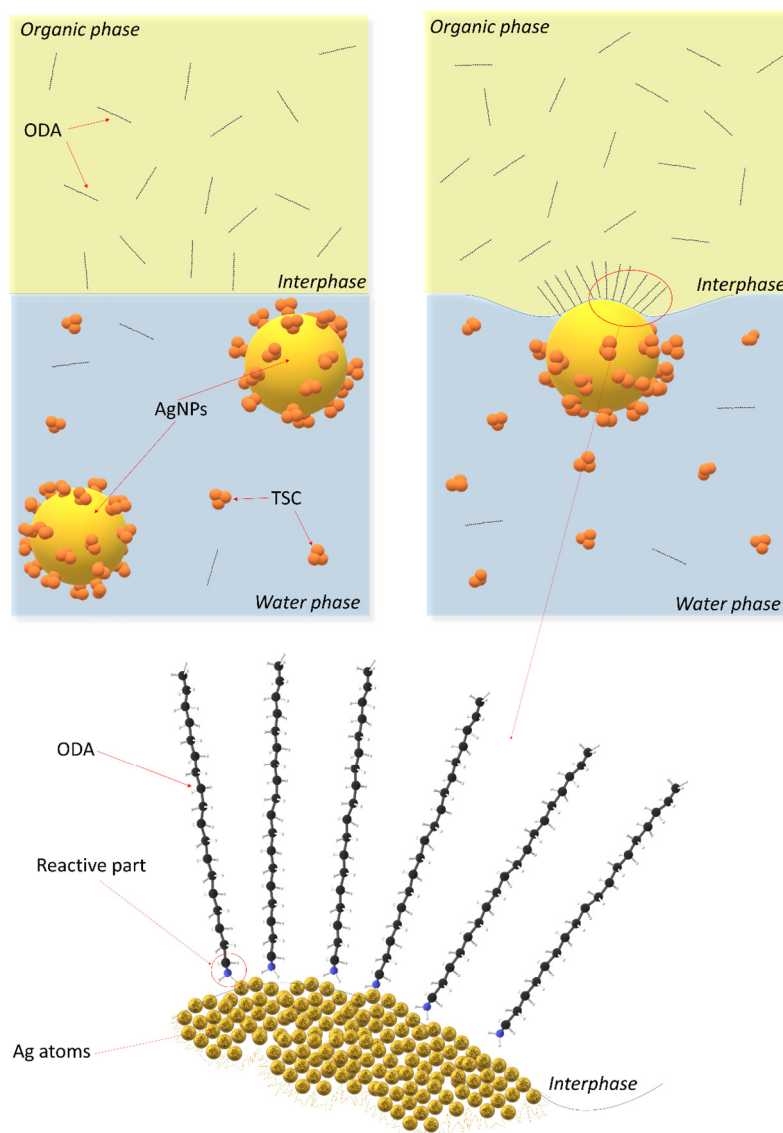
Figure 7. Scheme of AgNPs extraction.

The nanoparticle extraction process consists of chemical and physical processes. Physical processes include diffusion and transport of ODA particles and silver nanoparticles to the interface. Chemical processes include the creation of bonds between the active part of the ODA molecule and the silver atoms that are part of the silver nanoparticles. ODA is practically insoluble in aqueous solutions [46]. However, for extraction to occur, there must be minimal solubility of the ODA in the aqueous phase. ODA concentrated at the interface adsorbs on the surface of AgNPs. The nanoparticle is adsorbed at the interface and is held at this interface by ODA. At the same time, it is accompanied by limited Brownian motion and TSC desorption. AgNPs lose their surface charge, and gradually the degree of coverage of the nanoparticle surface by ODA increases. In the last step, it is completely transferred to the organic phase.

If the concentration of ODA in the organic phase is low, then the interface between the phases is not covered by ODA. The diffusion time of ODA from the organic phase is long, thus, particles partially deprived of the protective layer may collide at the phase boundary. We observe Ostwald ripening, coagulation, and growth of silver nanoparticles at the phase boundary. This explains why the concentration of ODA has a significant impact on the process. For different solvents, the ODA partition coefficient may be different. This also

explains why chloroform, and ethyl acetate, which dissolve ODA very well, are also poorly suited for the extraction of AgNPs.

3.6. XRD Analysis

It is typical for colloid XRD analyses that the signal-to-noise intensity is low. This is due to the fact that the number of planes in nanoparticles capable of reflecting X-rays is small in relation to the depth of penetration of the radiation. It is assumed that the penetration depth is about 5 μm. In the case of nanoparticles with 15 nm, it is over 300 times less. Therefore, such signals are always highly noisy. The recorded diffractograms are shown in Figure 8A,B.
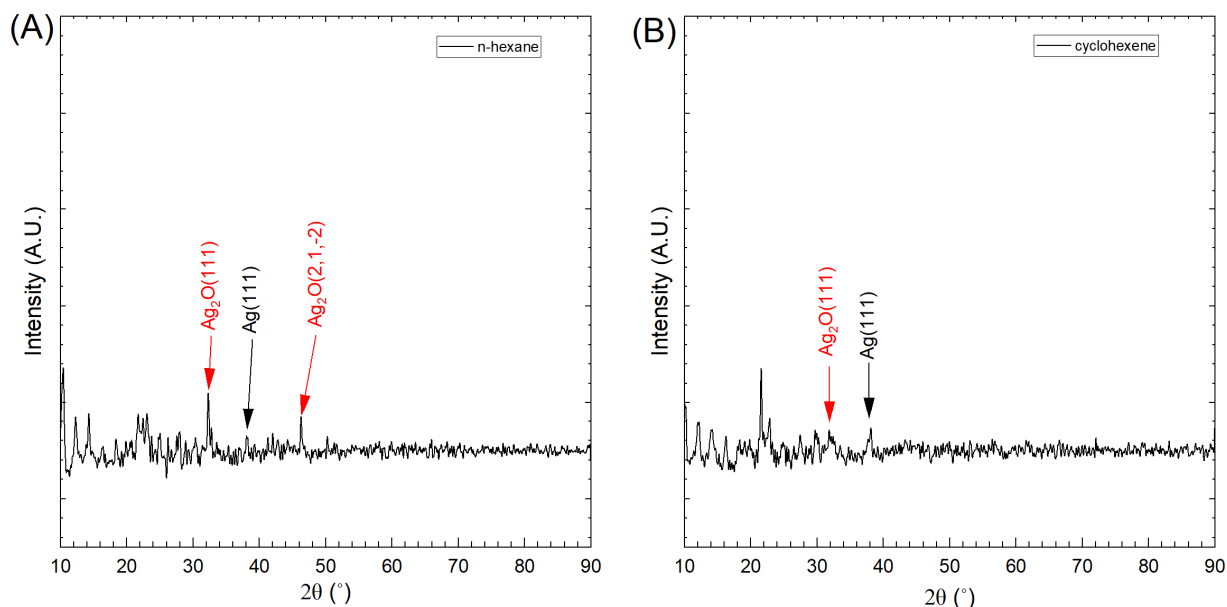

Figure 8. XRD analysis of AgNPs extracted to: n-hexane (**A**), and cyclohexene (**B**).

Both in the case of nanoparticles extracted into n-hexane and cyclohexane, the presence of an oxide phase was observed. The presence of strong surface plasmon resonance in the dispersed phase suggests that silver oxide formation is rather related to sample preparation for XRD measurements. During the evaporation of the organic phase, secondary oxidation of AgNPs occurred. In this type of preparation, it is not possible to quantify individual phases. The crystallographic structure can also be confirmed by HR-TEM analysis, which is described in the next section.

3.7. HR-TEM Analysis

HR-TEM analyses were performed for samples after extraction into the organic phase. One of the first observations is the lack of contamination of samples during the analysis, which is typical for high-resolution analyzes of preparations applied from the water phase. The number of particles allowed for their well-quality analysis. It is hypothesized that during the application of preparations from the water phase, nanoparticles tend to accumulate at the water-air interface during drying. Their high concentration is on the edge of the microscopic gratings, which are not analyzed by the TEM technique. In the case of applying preparations from the organic phase, they are quite evenly applied to the TEM grid membrane.

The images of AgNPs extracted to different organic phases are shown in Figure 9A,C,D. Figure 9B shows the results of the fast Fourier transform (FFT) analysis of selected nanoparticles. This analysis confirms the presence of Ag in the FCC (face-centered cubic) crystal structure.
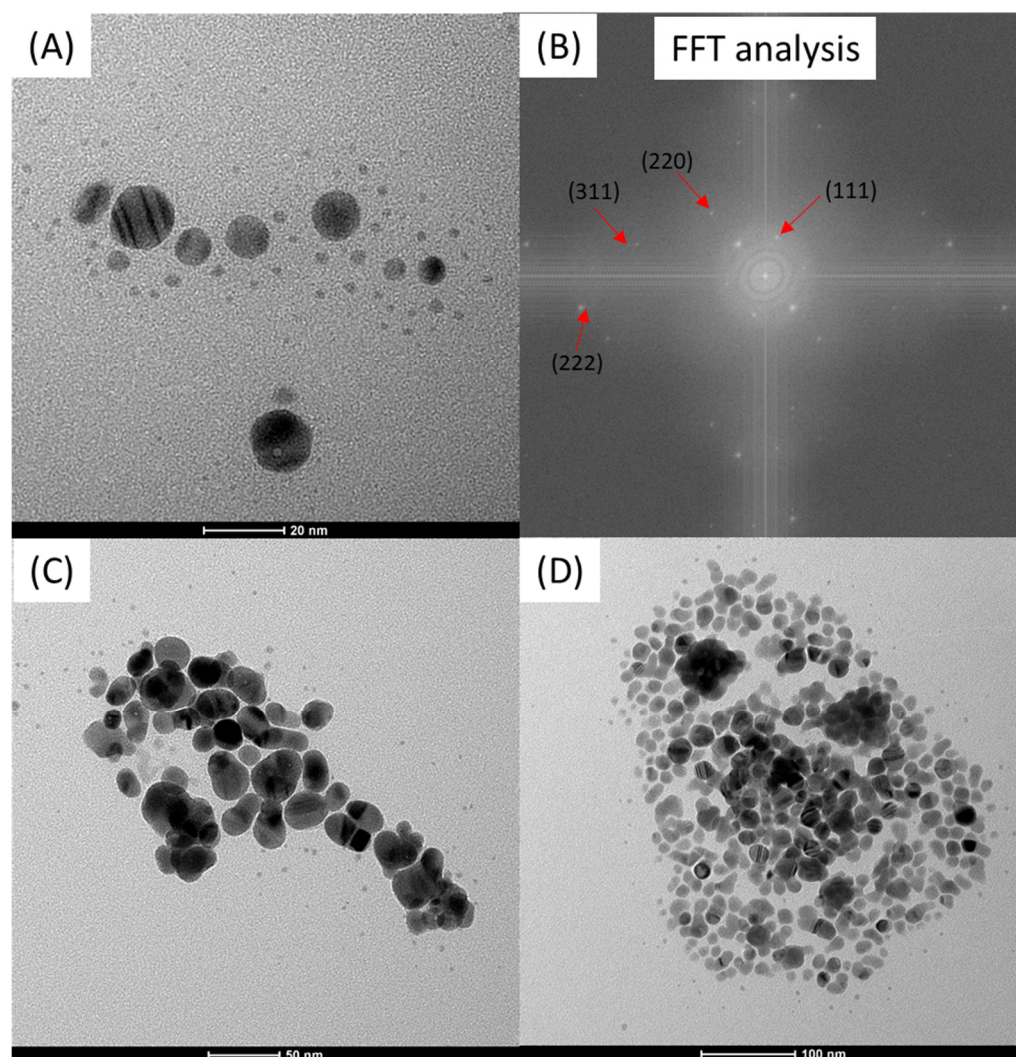
Figure 9. HR-TEM image of particles extracted to: (**A**) n-hexane, (**C**) cyclohexane, (**D**) toluene, and FFT analysis of selected nanoparticles extracted to (**B**) n-hexane.

It is worth noting that the silver nanoparticles that were extracted into the ODA solution in n-hexane had a regular, spherical shape, while the nanoparticles extracted into cyclohexane and toluene had a non-spherical shape. The variation in shape is only due to the use of different solvents for ODA. Wojnicki et al. [47] describe the influence of the dielectric permittivity of water on the shape of PtNPs obtained during chemical synthesis. Authors suggested that the adsorption of TSC (playing as a stabilizing agent) at the surface of PtNPs depends on dielectric constants. Additionally, the changes in dielectric constants change the solubility of TSC in water, affecting the adsorption process.

Therefore, analyses of a minimum of 100 particles were carried out to confirm whether the observation was actually a change in shape. For anisotropic nanoparticles, the diameter (d) and length (L) were measured. The results obtained are shown in Figure 10A–C.
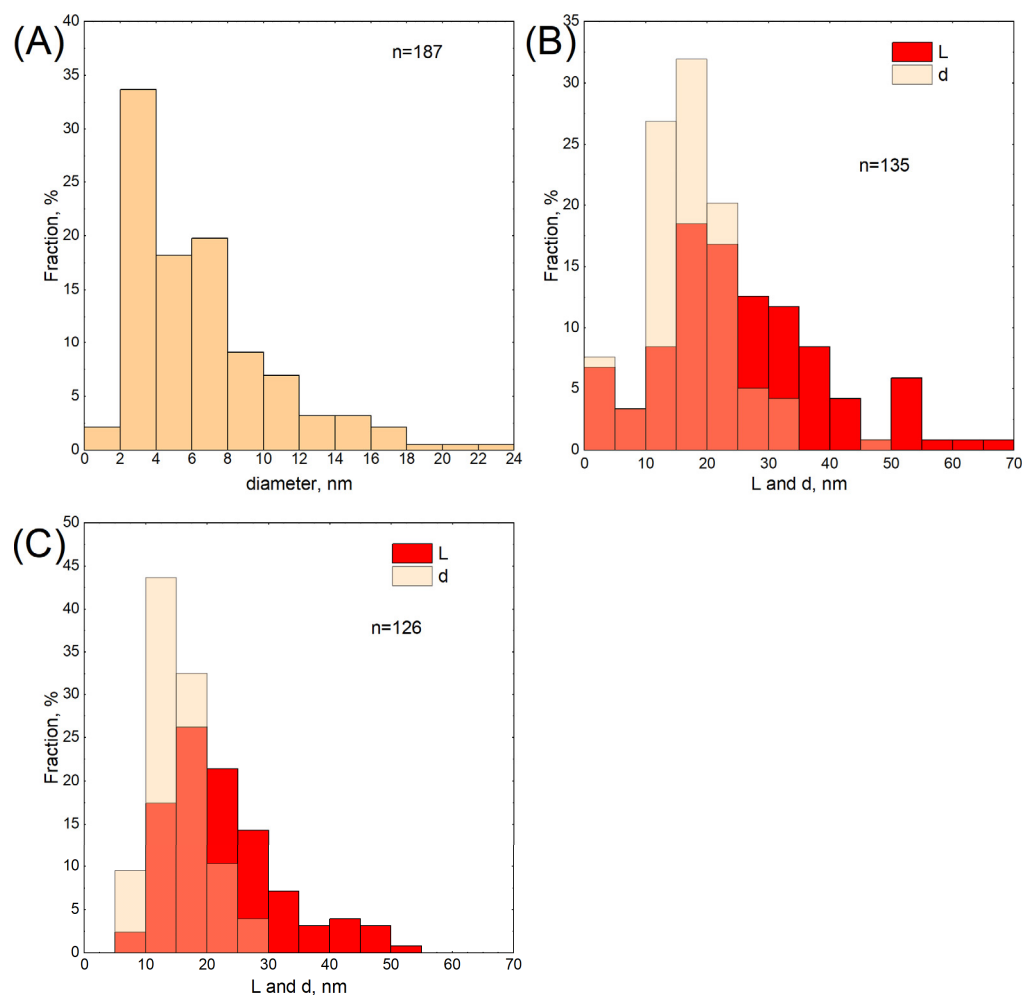
Figure 10. Particle size distribution extracted to various organic phases (**A**) n-hexane, (**B**) cyclohexene, (**C**) toluene.

Via DLS, it was identified that the hydrodynamic radius changes depending on the solvent used for the organic extraction phase. For anisotropic nanoparticles, the hydrodynamic radius is equivalent to the largest dimension of the particle. The radius change is, accordingly, not a result of a hard material-based aggregation, e.g., nanoparticle flocculation, but is hydrodynamically defined by a change of the "solvent cloud" around the nanoparticles when passing from one phase to another. While the UV-Vis results were indicative of a radius change (change in the position of the surface plasmon resonance peak maximum), the magnitude of this effect due to a mere interfacial transfer was not expected. This hypothesis and its experimental confirmation are reported here for the first time. Previous studies with silver colloids, taking into account the interfacial extraction of silver nanoparticles into the organic phase [39,48] or reactions in the formation of surface bonds of silver nanoparticles with chain organic compounds [49], do not report similar results.

Future investigations should reconsider the interfacial transfer and the reactions occurring at the interface from the viewpoint of the change of the hydrodynamic radius. The phenomena accompanying the transition of a nanoparticle from the aqueous phase to the organic phase, such as TSC desorption or ODA adsorption, probably involve several steps. This can affect the interaction between the individual nanoparticles, for example, when attractive forces become sufficiently strong to cause agglomeration. The solution to this problem is a proper choice of the organic solvent and its key property, which are the surface tension and the dielectric constant to define and stabilize the interface. Deciphering the mechanism of this interaction opens the door to future physico-chemical studies.

4. Conclusions

A series of tests were carried out to determine the conditions under which it is possible to extract silver nanoparticles from aqueous solutions into the organic phase using ODA as an interfacial transfer phase transfer agent. Preliminary studies have shown that the mechanism of nanoparticle transfer from the aqueous phase to the organic phase using ODA is complex and consists of several steps. As the first step, the Ag nanoparticles are transferred to the phase boundary. As the second step, the ODA molecules adsorb on the AgNPs surface. The spherical shape of the nanoparticle, meaning the small relative surface-to-volume ratio, reduces the amount of ODA surface coverage. If the diffusion rate of ODA to the interface surface is low (low initial concentration of ODA in the organic phase), the nanoparticle is trapped at the interface for a longer time. The chance of collision of Ag nanoparticles leading to Ostwald ripening is much higher at the interface than in the bulk of the solution. Our experimental results prove that this suggested mechanism is consistent with all achievements reported in this manuscript. Advanced in-situ phase boundary analysis will be used to elucidate further and reassure this mechanism.

The best results were obtained for hexane and cyclohexane as a solvent for the organic phase. The studies on the influence of ODA initial concentration and organic-water phase ratio lead to the following conclusions:

- At the phase boundary, the process of ODA adsorption on the surface of silver nanoparticles takes place.
- Low concentration of ODA in the organic phase results in the formation of the third phase or a complete lack of extraction of silver nanoparticles.

These analyses lead to the conclusion that within a few seconds of extraction, it is possible to increase the concentration of colloids in solutions by 500 times. In the extreme case, the concentration of silver nanoparticles increased from 5×10^{-4} M to 0.25 M. There are only a few reports on the single-step synthesis of AgNPs compared to high concentrations. Wojnicki et al. [25] obtained a 0.05 M concentration of AgNPs in the water phase directly using L-cysteine as a stabilizing agent and borane dimethylamine complex as a reducing agent. Yang et al. [50] showed that it is possible to obtain a high concentration of more than 2 mg/mL of AgNPs. This value is a ten times higher concentration than in our case. Optimization combined with the evaporation of n-hexane may allow the synthesis of much more concentrated colloids.

The ODA was found as a promising tool for an effective synthesis for the preparation of various nanocrystals, including metals, mixed metal oxides, metal/metal oxide hetero-structured nanocrystals, intermetallic, and alloys were presented [51]. The formation of close-packed silver nanoparticle thin films via a two-stage self-assembly approach was described by Vijaya Patil and Murali Sastry using ODA [52]. Unfortunately, the presented obtained materials are no longer in the colloidal phase.

The fact that reactions taking place at the phase boundary cause changes in the shape of nanoparticles sheds new light on the potential applications of this phenomenon. Shape-selective synthesis of nanoparticles is still a challenge in colloid preparation and is being intensively developed [53–56]. It should be considered whether the appropriate selection of phases and phase modifiers will not provide new possibilities for the synthesis of nanoparticles of various shapes.

Author Contributions: Conceptualization, M.W.; Validation, R.P.S.; Investigation, K.W., T.T., D.K. and K.K.-S.; Resources, P.Ż.; Writing—original draft, E.C., M.E.-G. and M.W.; Writing—review & editing, V.H. and M.W. All authors have read and agreed to the published version of the manuscript.

Institutional Review Board Statement: Not applicable.

Informed Consent Statement: Not applicable.

References

1. Yusuf, M. Silver Nanoparticles: Synthesis and Applications. In *Handbook of Ecomaterials*; Martínez, L.M.T., Kharissova, O.V., Kharisov, B.I., Eds.; Springer International Publishing: Cham, Switzerland, 2019; pp. 2343–2356.
2. Iravani, S.; Korbekandi, H.; Mirmohammadi, S.V.; Zolfaghari, B. Synthesis of silver nanoparticles: Chemical, physical and biological methods. *Res. Pharm. Sci.* **2014**, *9*, 385–406.
3. Gudikandula, K.; Maringanti, S.C. Synthesis of silver nanoparticles by chemical and biological methods and their antimicrobial properties. *J. Exp. Nanosci.* **2016**, *11*, 714–721. [CrossRef]
4. Xiao, Q.; Yao, Z.; Liu, J.; Hai, R.; Oderji, H.Y.; Ding, H. Synthesis and characterization of Ag–Ni bimetallic nanoparticles by laser-induced plasma. *Thin Solid Films* **2011**, *519*, 7116–7119. [CrossRef]
5. Asanithi, P.; Chaiyakun, S.; Limsuwan, P. Growth of Silver Nanoparticles by DC Magnetron Sputtering. *J. Nanomater.* **2012**, *2012*, 963609. [CrossRef]
6. Jabłońska, J.; Jankowski, K.; Tomasik, M.; Cykalewicz, D.; Uznański, P.; Całuch, S.; Szybowicz, M.; Zakrzewska, J.; Mazurek, P. Preparation of silver nanoparticles in a high voltage AC arc in water. *SN Appl. Sci.* **2021**, *3*, 244. [CrossRef]
7. Wojnicki, M.; Mania, I.; Marzec, M.; Gajewska, M.; Mech, K. Influence of experimental conditions on deposition of silver nanoparticles onto surface of graphene oxide. *Arch. Metall. Mater.* **2015**, *60*, 2631–2635. [CrossRef]
8. Özkar, S.; Finke, R.G. Silver Nanoparticles Synthesized by Microwave Heating: A Kinetic and Mechanistic Re-Analysis and Re-Interpretation. *J. Phys. Chem. C* **2017**, *121*, 27643–27654. [CrossRef]
9. Pal, A.; Shah, S.; Devi, S. Microwave-assisted synthesis of silver nanoparticles using ethanol as a reducing agent. *Mater. Chem. Phys.* **2009**, *114*, 530–532. [CrossRef]
10. Zhao, X.; Xia, Y.; Li, Q.; Ma, X.; Quan, F.; Geng, C.; Han, Z. Microwave-assisted synthesis of silver nanoparticles using sodium alginate and their antibacterial activity. *Colloids Surf. A Physicochem. Eng. Asp.* **2014**, *444*, 180–188. [CrossRef]
11. Tuleshova, E.Z.; Baeshov, A.B. Electrochemical method for obtaining a finely dispersed silver powder. *Russ. J. Appl. Chem.* **2015**, *88*, 1142–1145. [CrossRef]
12. Jara, N.; Milán, N.S.; Rahman, A.; Mouheb, L.; Boffito, D.C.; Jeffryes, C.; Dahoumane, S.A. Photochemical Synthesis of Gold and Silver Nanoparticles—A Review. *Molecules* **2021**, *26*, 4585. [CrossRef] [PubMed]
13. Pascu, B.; Negrea, A.; Ciopec, M.; Duteanu, N.; Negrea, P.; Bumm, L.A.; Grad, O.; Nemeş, N.S.; Mihalcea, C.; Duda-Seiman, D.M. Silver Nanoparticle Synthesis via Photochemical Reduction with Sodium Citrate. *Int. J. Mol. Sci.* **2023**, *24*, 255. [CrossRef]
14. Zhang, Y.; Chen, F.; Zhuang, J.; Tang, Y.; Wang, D.; Wang, Y.; Dong, A.; Ren, N. Synthesis of silver nanoparticles via electrochemical reduction on compact zeolite film modified electrodes. *Chem. Commun.* **2002**, *23*, 2814–2815. [CrossRef] [PubMed]
15. Kuntyi, O.; Mazur, A.; Kytsya, A.; Karpenko, O.; Bazylyak, L.; Mertsalo, I.; Pokynbroda, T.; Prokopalo, A. Electrochemical synthesis of silver nanoparticles in solutions of rhamnolipid. *Micro Nano Lett.* **2020**, *15*, 802–807. [CrossRef]
16. Singaravelan, R.; Bangaru Sudarsan Alwar, S. Electrochemical synthesis, characterisation and phytogenic properties of silver nanoparticles. *Appl. Nanosci.* **2015**, *5*, 983–991. [CrossRef]
17. Mavaei, M.; Chahardoli, A.; Shokoohinia, Y.; Khoshroo, A.; Fattahi, A. One-step Synthesized Silver Nanoparticles Using Isoimperatorin: Evaluation of Photocatalytic, and Electrochemical Activities. *Sci. Rep.* **2020**, *10*, 1762. [CrossRef]
18. Mavani, K.; Shah, M. Synthesis of Silver Nanoparticles by Using Sodium Borohydride as a Reducing Agent. *Int. J. Eng. Res. Technol.* **2013**, *2*, 1–5. [CrossRef]
19. Quintero-Quiroz, C.; Acevedo, N.; Zapata-Giraldo, J.; Botero, L.E.; Quintero, J.; Zárate-Triviño, D.; Saldarriaga, J.; Pérez, V.Z. Optimization of silver nanoparticle synthesis by chemical reduction and evaluation of its antimicrobial and toxic activity. *Biomater. Res.* **2019**, *23*, 27. [CrossRef]
20. Mushran, S.P.; Agrawal, M.C.; Mehrotra, R.M.; Sanehi, R. Kinetics and Mechanism of Reduction of Silver(I) by Ascorbic Acid. *J. Chem. Soc. Dalton Trans.* **1973**, *3*, 1460–1462. [CrossRef]
21. Malassis, L.; Dreyfus, R.; Murphy, R.J.; Hough, L.A.; Donnio, B.; Murray, C.B. One-step green synthesis of gold and silver nanoparticles with ascorbic acid and their versatile surface post-functionalization. *RSC Adv.* **2016**, *6*, 33092–33100. [CrossRef]
22. Katherine, G.; Brajesh, K.; Marcelo, G.; Alexis, D.; Luis, C. Ascorbic Acid-assisted Green Synthesis of Silver Nanoparticles: pH and Stability Study. In *Green Chemistry*; Brajesh, K., Alexis, D., Eds.; IntechOpen: Rijeka, Croatia, 2022; Chapter 13. [CrossRef]
23. Zain, N.M.; Stapley, A.G.F.; Shama, G. Green synthesis of silver and copper nanoparticles using ascorbic acid and chitosan for antimicrobial applications. *Carbohydr. Polym.* **2014**, *112*, 195–202. [CrossRef] [PubMed]
24. Eka Putri, G.; Rahayu Gusti, F.; Novita Sary, A.; Zainul, R. Synthesis of silver nanoparticles used chemical reduction method by glucose as reducing agent. *J. Phys. Conf. Ser.* **2019**, *1317*, 012027. [CrossRef]

25. Wojnicki, M.; Luty-Błocho, M.; Kotańska, M.; Wytrwal, M.; Tokarski, T.; Krupa, A.; Kołaczkowski, M.; Bucki, A.; Kobielusz, M. Novel and effective synthesis protocol of AgNPs functionalized using L-cysteine as a potential drug carrier. *Naunyn-Schmiedeberg's Arch. Pharmacol.* **2018**, *391*, 123–130. [CrossRef] [PubMed]

26. Babu Kalidindi, S.; Sanyal, U.; Jagirdar, B.R. Chemical Synthesis of Metal Nanoparticles Using Amine–Boranes. *ChemSusChem* **2011**, *4*, 317–324. [CrossRef] [PubMed]

27. Agnihotri, S.; Mukherji, S.; Mukherji, S. Size-controlled silver nanoparticles synthesized over the range 5–100 nm using the same protocol and their antibacterial efficacy. *RSC Adv.* **2014**, *4*, 3974–3983. [CrossRef]

28. Wang, X.; Zhao, Z.; Ou, D.; Tu, B.; Cui, D.; Wei, X.; Cheng, M. Size-controlled synthesis of silver nanoparticles from silver mirror reaction in toluene. *Micro Nano Lett.* **2016**, *11*, 454–456. [CrossRef]

29. Zhang, W.; Zhang, L.; Sun, Y. Size-controlled green synthesis of silver nanoparticles assisted by L-cysteine. *Front. Chem. Sci. Eng.* **2015**, *9*, 494–500. [CrossRef]

30. Gul, N.; Ata, S.; Bibi, I.; Ijaz ul, M.; Azam, M.; Shahid, A.; Alwadai, N.; Masood, N.; Iqbal, M. Size controlled synthesis of silver nanoparticles: A comparison of modified Turkevich and BRUST methods. *J. Phys. Chem.* **2022**, *236*, 1173–1189. [CrossRef]

31. Dong, X.; Ji, X.; Wu, H.; Zhao, L.; Li, J.; Yang, W. Shape Control of Silver Nanoparticles by Stepwise Citrate Reduction. *J. Phys. Chem. C* **2009**, *113*, 6573–6576. [CrossRef]

32. Khodashenas, B.; Ghorbani, H.R. Synthesis of silver nanoparticles with different shapes. *Arab. J. Chem.* **2019**, *12*, 1823–1838. [CrossRef]

33. Mukherji, S.; Bharti, S.; Shukla, G.; Mukherji, S. Synthesis and characterization of size- and shape-controlled silver nanoparticles. *Phys. Sci. Rev.* **2019**, *4*, 20170082. [CrossRef]

34. Hong, T.; Lu, A.; Liu, W.; Chen, C. Microdroplet Synthesis of Silver Nanoparticles with Controlled Sizes. *Micromachines* **2019**, *10*, 274. [CrossRef] [PubMed]

35. Zhu, J.; Liu, S.; Palchik, O.; Koltypin, Y.; Gedanken, A. Shape-Controlled Synthesis of Silver Nanoparticles by Pulse Sonoelectrochemical Methods. *Langmuir* **2000**, *16*, 6396–6399. [CrossRef]

36. Martins, C.S.M.; Sousa, H.B.A.; Prior, J.A.V. From Impure to Purified Silver Nanoparticles: Advances and Timeline in Separation Methods. *Nanomaterials* **2021**, *11*, 3407. [CrossRef] [PubMed]

37. Alele, N.; Streubel, R.; Gamrad, L.; Barcikowski, S.; Ulbricht, M. Ultrafiltration membrane-based purification of bioconjugated gold nanoparticle dispersions. *Sep. Purif. Technol.* **2016**, *157*, 120–130. [CrossRef]

38. Wang, X.; Xu, S.; Zhou, J.; Xu, W. A rapid phase transfer method for nanoparticles using alkylamine stabilizers. *J. Colloid Interface Sci.* **2010**, *348*, 24–28. [CrossRef]

39. Kumar, A.; Joshi, H.; Pasricha, R.; Mandale, A.B.; Sastry, M. Phase transfer of silver nanoparticles from aqueous to organic solutions using fatty amine molecules. *J. Colloid Interface Sci.* **2003**, *264*, 396–401. [CrossRef]

40. Sastry, M. Phase transfer protocols in nanoparticle synthesis. *Curr. Sci.* **2003**, *85*, 1735–1745.

41. Smits, J.; Giri, R.P.; Shen, C.; Mendonça, D.; Murphy, B.; Huber, P.; Rezwan, K.; Maas, M. Synergistic and Competitive Adsorption of Hydrophilic Nanoparticles and Oil-Soluble Surfactants at the Oil–Water Interface. *Langmuir* **2021**, *37*, 5659–5672. [CrossRef]

42. Benitez, J.J.; Fuente, O.R.d.l.; Díez-Pérez, I.; Sanz, F.; Salmeron, M. Dielectric properties of self-assembled layers of octadecylamine on mica in dry and humid environments. *J. Chem. Phys.* **2005**, *123*, 104706. [CrossRef]

43. Bossa, G.V.; Roth, J.; Bohinc, K.; May, S. The apparent charge of nanoparticles trapped at a water interface. *Soft Matter* **2016**, *12*, 4229–4240. [CrossRef] [PubMed]

44. Wyman, J. The dielectric constant of mixtures of ethyl alcohol and water from −5 to 40°. *J. Am. Chem. Soc.* **1931**, *53*, 3292–3301. [CrossRef]

45. Elliott, N.B.; Prenni, A.J.; Ndou, T.T.; Warner, I.M. Size-Selective Extraction of Polycyclic Aromatic Hydrocarbons from a Microemulsion System Using Cyclodextrins. *J. Colloid Interface Sci.* **1993**, *156*, 359–364. [CrossRef]

46. National Center for Biotechnology Information. 2023. Available online: https://pubchem.ncbi.nlm.nih.gov/compound/Octadecylamine (accessed on 12 February 2023).

47. Wojnicki, M.; Luty-Błocho, M.; Kwolek, P.; Gajewska, M.; Socha, R.P.; Pędzich, Z.; Csapó, E.; Hessel, V. The influence of dielectric permittivity of water on the shape of PtNPs synthesized in high-pressure high-temperature microwave reactor. *Sci. Rep.* **2021**, *11*, 4851. [CrossRef] [PubMed]

48. Machunsky, S.; Peuker, U.A. Liquid-Liquid Interfacial Transport of Nanoparticles. *Phys. Sep. Sci. Eng.* **2007**, *2007*, 034832. [CrossRef]

49. Sredojević, D.; Stavrić, S.; Lazić, V.; Ahrenkiel, S.P.; Nedeljković, J.M. Interfacial charge transfer complex formation between silver nanoparticles and aromatic amino acids. *Phys. Chem. Chem. Phys.* **2022**, *24*, 16493–16500. [CrossRef]

50. Yang, J.; Yin, H.; Jia, J.; Wei, Y. Facile Synthesis of High-Concentration, Stable Aqueous Dispersions of Uniform Silver Nanoparticles Using Aniline as a Reductant. *Langmuir* **2011**, *27*, 5047–5053. [CrossRef]

51. Wang, D.; Li, Y. Effective Octadecylamine System for Nanocrystal Synthesis. *Inorg. Chem.* **2011**, *50*, 5196–5202. [CrossRef]

52. Patil, V.; Sastry, M. Formation of Close-Packed Silver Nanoparticle Multilayers from Electrostatically Grown Octadecylamine/Colloid Nanocomposite Precursors. *Langmuir* **2000**, *16*, 2207–2212. [CrossRef]

53. Yin, A.-X.; Min, X.-Q.; Zhang, Y.-W.; Yan, C.-H. Shape-Selective Synthesis and Facet-Dependent Enhanced Electrocatalytic Activity and Durability of Monodisperse Sub-10 nm Pt−Pd Tetrahedrons and Cubes. *J. Am. Chem. Soc.* **2011**, *133*, 3816–3819. [CrossRef]

54. Kundu, S.; Liang, H. Photoinduced Formation of Shape-Selective Pt Nanoparticles. *Langmuir* **2010**, *26*, 6720–6727. [CrossRef] [PubMed]
55. Gupta, S.S.R.; Kantam, M.L.; Bhanage, B.M. Shape-selective synthesis of gold nanoparticles and their catalytic activity towards reduction of p-nitroaniline. *Nano-Struct. Nano-Objects* **2018**, *14*, 125–130. [CrossRef]
56. Yamashita, Y.; Tashiro, S.; Ishii, Y.; Uchihashi, T.; Matsushita, N.; Kubota, R.; Shionoya, M. Shape-selective one-step synthesis of branched gold nanoparticles on the crystal surface of redox-active PdII-macrocycles. *Dalton Trans.* **2022**, *51*, 1318–1324. [CrossRef] [PubMed]